Available online at www.sciencedirect.com
SCIENCE DIRECT®
Journal of Power Sources 133 (2004) 205–213
JOURNAL OF POWER SOURCES
www.elsevier.com/locate/jpowsour

Investigation of reactant transport within a polymer electrolyte fuel cell using localised CO stripping voltammetry and adsorption transients

D.J.L. Brett [a], S. Atkins [a], N.P. Brandon [b], V. Vesovic [c], N. Vasileiadis [b], A.R. Kucernak [a,*]

[a] *Department of Chemistry, Imperial College London, London SW7 2AZ, UK*
[b] *Department of Chemical Engineering, Imperial College London, London SW7 2AZ, UK*
[c] *Department of Earth Science and Engineering, Imperial College London, London SW7 2AZ, UK*

Received 14 November 2003; received in revised form 2 February 2004; accepted 9 February 2004

Available online 13 April 2004

Abstract

The distribution of carbon monoxide (CO) within a simple one dimensional polymer electrolyte fuel cell (PEFC) is studied experimentally using localised stripping voltammetry and adsorption transients. The effect of varying the carrier gas flow rate and CO dosage is investigated. It is found that residence time within the fuel cell is the key factor in determining the extent of poisoning or CO adsorption. Low flow rates are seen to result in a more anisotropic distribution of CO with greater amounts found away from the channel. High flow rates lead to a much more uniform profile. Diffusion of reactant into the gas distribution layer (GDL) and adsorption onto the catalyst retards the flow of reactant down the channel which broadens the peak width of the bulk adsorption transient. With knowledge of the catalyst roughness factor, pseudo 2-D reactant distribution profiles can be derived. These diagrams provide the equivalent of 'snap-shots' of the flow of reactants through the simple one dimensional fuel cell. This technique has applications in optimising the lateral distribution of catalyst and MEA properties such as GDL porosity.

Keywords: Polymer electrolyte fuel cell; CO stripping; Reactant distribution; Adsorption transient

1. Introduction

Polymer electrolyte fuel cells (PEFC) represent a highly promising technology for widespread use as an energy conversion device. The scope of application ranges from small mobile electronic devices, through automotive traction to large scale residential power generation. The potential market for such devices is huge, and the success of the technology could inspire a paradigm shift in the way we use energy, encouraging a retreat from our reliance on fossil fuels and moving to the vision of a 'hydrogen economy' [1]. Efforts to improve fuel cell systems constitute a vast area of research. The effectiveness of new techniques and materials can only be appreciated by careful measurement of the parameters that characterise fuel cell performance. Understanding how a fuel cell operates internally is of vital importance in optimising such a system, especially since so many parameters can affect their operation. We have found that one of the most effective methods of determining how a fuel cell is performing is by making localised measurements of parameters such as current density, contact resistance, membrane conductance and impedance [2,3]. The importance of localised measurements have been realised by other workers, and the repertoire of techniques continues to grow [4–9]. The work presented here, aims to establish a new technique of spatial visualisation in which the distribution of an adsorbed species is determined by localised adsorption transients and localised electrochemical stripping. Representative data is included for carbon monoxide (CO) at a range of flow rates and dosing levels. CO is studied for two reasons; firstly, CO is a poison to fuel cells and as such its distribution is of obvious interest; secondly, CO is an ideal probe of the way in which reactant flows in the channel and in the gas diffusion layer (GDL). Such a probe technique is envisaged to serve as a useful tool for flow-field design.

The ability of the PEFC to operate at relatively low temperatures (room temperature to 90 °C unpressurised) and achieve high current density makes it ideally applicable to mobile and automotive applications. Hydrogen is the fuel gas of choice for the PEFC. However, an adequate distribution network or efficient method of storage has yet to be established. At present, the most cost effective method of

* Corresponding author. Tel.: +44-20-75945831; fax: +44-20-75945804.
E-mail address: a.kucernak@imperial.ac.uk (A.R. Kucernak).

0378-7753/$ – see front matter © 2004 Elsevier B.V. All rights reserved.
doi:10.1016/j.jpowsour.2004.02.007

hydrogen generation is by reforming hydrocarbons [10]. This technology is well advanced, but the process outputs a product that contains an appreciable quantity of CO (typically 0.5–3%). Much of the CO produced in the steam reforming process can be converted subsequently to CO_2 in a shift reactor [11] reducing the CO concentration to the order of <1%. Techniques such as oxygen bleed [12] can minimise the effect of the CO further by reacting it with oxygen at catalyst sites within the fuel cell. However, in practice, hydrogen derived from the reforming of hydrocarbons will always contain some CO. To complicate matters, the amount of CO entering the fuel cell is liable to change during the course of operation, for example, during the start-up process or under severe load the reformer may expel 'burps' of CO. Such transients represent a serious threat to the efficient running of the fuel cell. Methods to accurately predict and determine the extent and location of catalyst poisoning would be of obvious use; and it is for this reason that we have developed the technique presented herein.

Since the concentration of CO entering the fuel cell will be very low (typically <100 ppm under stable operation) or as a transitory pulse, the effect of poisoning will tend to be heterogeneously distributed throughout the fuel cell, some parts experiencing a significantly greater concentration while other areas remaining unaffected. As such, a MEA could benefit from lateral engineering of the quantity and type of catalyst used. To date, efforts to improve catalyst efficiency have concentrated almost entirely on the nature of the catalyst, its morphology, method of support and dispersion and its integration with the electrolyte. However, very little attention has been paid to the macroscopic dispersion of the catalyst across the whole of the electrode. A notable exception is the work of Wilkinson and St-Pierre [13] which showed that varying the loading of catalyst spatially across the surface of the electrode can improve performance by complimenting the natural gradients of quantities such as humidity, temperature and reactant concentration, typically found in a fuel cell. It can be envisaged that an analogous distribution could be employed to manage CO poisoning such that a different type of catalyst or composition is deposited at locations that suffer most from poisoning.

Despite substantial work directed at improving catalyst and membrane technology, there is only a modest body of literature published on the subject of flow-field design [14–17]. This is disappointing, since many of the advantages gained from using advanced catalysts and optimised humidification regimes will be lost if good flow-field design is neglected. The flow-field plays several roles in the operation of a fuel cell. It must deliver reactant to the MEA; conduct current, make good electrical contact with the GDL and dissipate heat from the MEA. Physically the flow plate should be an excellent electrical conductor; impermeable to reactant, corrosion resistant; easily machined, conducive to fabrication of narrow repeat lengths, light weight and inexpensive. The key to good flow-plate design is optimising the channel to rib-landing space so as to maximise electrical conductivity (typically by increasing the contact with the GDL) and the accessibility of the available reactant to the catalyst (typically achieved by increasing the channel width). Clearly, these two requirements are conflicting and a compromise must be made, though this design compromise also needs to consider the characteristics of the GDL By virtue of the porosity of the GDL, reactant is allowed to diffuse under the rib-landings thereby maximising the catalyst availability and the contact area between the electrode and the flow plate. Despite the assistance to reactant distribution that the GDL confers, rib/channel optimisation is still an important issue. In fact, the presence of the GDL makes it more difficult to assess which parts of the catalyst layer the reactant is accessing. Therefore, the facility to practically determine exactly where reactant (or poison) is accessing the catalyst would be a boon for flow-plate design, and act as a tool to validate computer simulations of reactant transport within operating fuel cells.

2. Experimental

2.1. Materials and equipment

Membrane electrode assemblies (MEA) were composed of Nafion® 112 and Toray™ gas diffusion layers (TGP-H-060), and had an active area of 4 cm × 12 cm. The cathode side contained 0.38 mg cm^{-2} Pt, and the anode contained 0.4 mg cm^{-2} Pt/0.2 mg cm^{-2} Ru. The MEA was provided by Johnson Matthey (Sonning Common, UK). Gas humidification was performed using a Nafion® moisture exchange column (Omnifit, Cambridge, UK) capable of 100% relative humidity over the temperature range 30–80 °C for the flow rates used. Hydrogen, nitrogen, and carbon monoxide were research grade (>99.99%, BOC, UK). Mass flow controllers were used to control the gas flow rate (EL-FLOW, Bronkhorst B.V., The Netherlands). The fuel cell temperature was controlled using a PID temperature controller (Micro-Infinity™, Newport Electronics, USA) driving 4 × 25 W low-voltage heating elements (Cooper Tools GmbH, Germany). The fuel cell measurements were performed using ten in-house developed potentiostat-loads, each of which had a maximum current rating of 0.7 A. Control and data collection was performed using in-house developed LabVIEW™ programs (National Instruments, Texas, USA). The printed circuit board used to demarcate the channel and collect the current had a 200 μm feature resolution. The contacts collecting the current bridged the channel and were 1.1 cm long (in the direction parallel to the channel) and 0.8 cm wide (on each side of the channel in the direction perpendicular to the channel). The electrodes were gold plated.

Current collection on the opposite side of the MEA was performed using machined 'bubble tight' phenolic resin impregnated graphite (Le Carbone Ltd. (Great Britain)). Reactants on this side of the MEA flowed through multiple

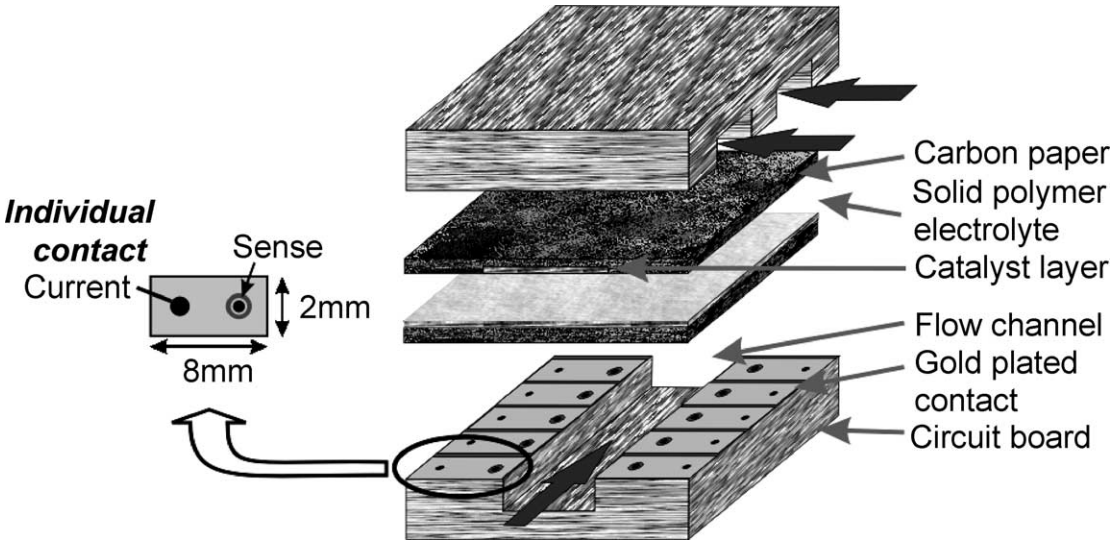

Fig. 1. Diagram of the channel flow and contact board configuration. CO dosing is imposed to the single linear channel. Individual current contacts are shown to either side of this channel. Hydrogen is supplied to the opposite electrode in a cross-flow configuration.

1 mm wide channels in a direction at right angles to the single channel. The MEA was gasketed using 150 μm thick Syndev® Silicone sheeting (Synergy Devices Ltd., UK). All measurements were performed at 25 °C.

2.2. Fuel cell configuration

The fuel cell system used was essentially the same as that described in previous papers [2,3], and is shown in schematic form in Fig. 1. In essence, the counter electrode side is supplied with hydrogen gas (100% relative humidity) via a cross-flow configuration that is machined into a graphite plate. This cross-flow configuration means that the hydrogen flows through multiple channels in a direction perpendicular to the single channel down which the air flows. Thus, the composition and properties of the anode gas is invariant with position, and any variation in local current density is determined by the rate of electrochemical reaction in the catalyst layer on the single channel side of the fuel cell. As the local current densities are always low, and IR effects are thus negligible, the counter electrode acts as a combined counter/reference electrode and all potentials are quoted versus the RHE.

Nitrogen is supplied to the working electrode side (dry) via a single channel that is 110 mm long, 1 mm wide and 1 mm deep. In typical fuel cell systems the performance of a fuel cell is measured by providing a variable load into which the fuel cell is coupled. The total current is the control variable, and the cell potential is the measured parameter. In our case, we control the cell potential and measure the local current. We do this to be assured that we are measuring a local current. This approach is very similar to that in operation in a potentiostat. In our case the potential of the local contact to the MEA is driven by separate electronic potentiostat/load circuits to a potential such that the voltage measured by a sense contact at that local point on the MEA equals the set potential. This approach provides dynamic compensation for all electronic IR losses (i.e. in cables and at the MEA/contact interface). The system does not require a segmented MEA, as each contact drives local regions of the MEA to the same potential and thus there is no lateral flow of current due to potential gradients.

2.3. CO distribution measurements

Before each CO distribution measurement a background voltammogram of the electrode was performed at a scan rate of 10 mV s^{-1}, this ensures that the surface is devoid of any CO and allows the catalyst surface area to be determined. It also ensures that the state of the catalyst electrode does not vary over the course of the experiment. CO was dosed into the system by using a gas syringe to inject a known quantity of CO 4 cm before the start of the channel, whilst a constant flow of nitrogen flowed through the channel. The injection is made through a septum and the tip of the syringe was at the same position each time. Dosing was made 5 s after the start of data acquisition and performed manually in a single rapid action. During the CO adsorption process the electrode was polarised at 90 mV (RHE)—within the potential range of hydrogen adsorption. Adsorption of CO at this potential results in a displacement current due to the oxidation of adsorbed hydrogen as it is displaced by CO (see below). After a suitable period had elapsed, the potential was scanned positive at 10 mV s^{-1} to a potential of 0.9 V. This scan rate was used to reduce the current density so as to minimise polarisation of the hydrogen reference electrode/counter electrode and to represent a situation close to equilibrium at each potential. The entire process is shown schematically in Fig. 2(a).

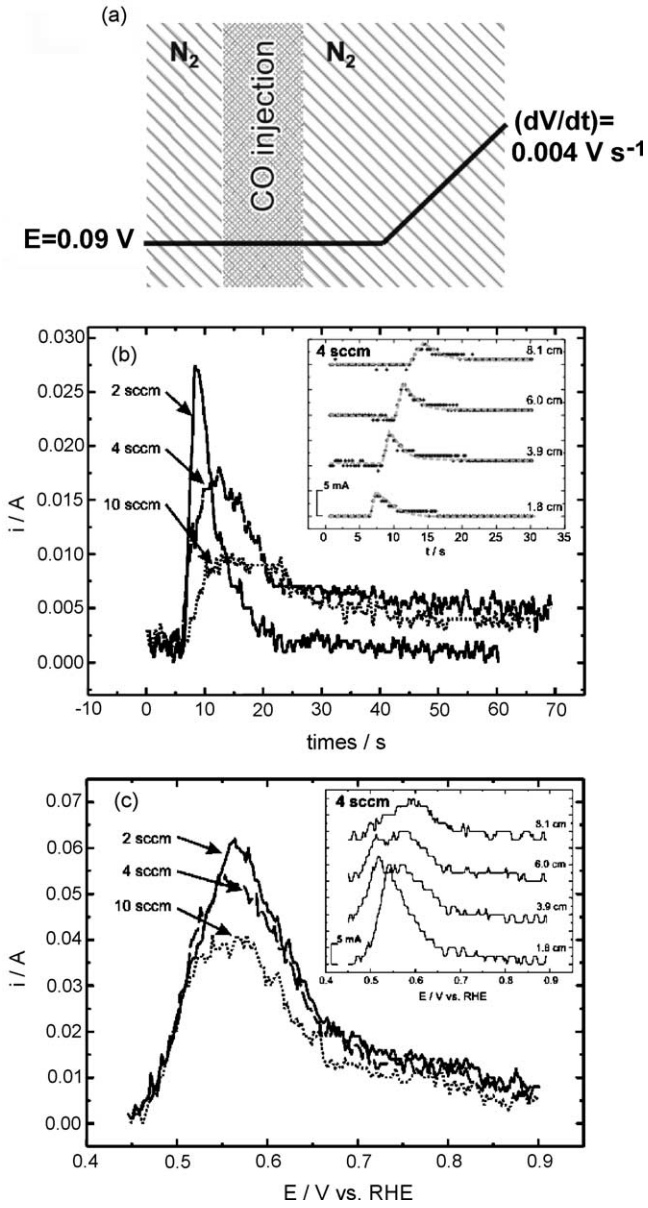

Fig. 2. (a) Diagram showing CO dosing and stripping program. (b) Total transient current for CO adsorption at carrier gas flow rates of 2, 4 and 10 sccm; inset are the localised current transients at 1.8, 3.9, 6.0 and 8.1 cm along the channel at a flow rate of 4 sccm (currents are offset up the *y*-axis for clarity). (c) Total CO stripping current at a carrier gas flow rate of 2, 4, and 10 sccm, scan rate 0.004 V s^{-1}; inset are the localised CO stripping currents at 1.8, 3.9, 6.0 and 8.1 cm along the channel for a flow rate of 4 sccm (currents are offset up the *y*-axis for clarity).

After the CO had been oxidised, the potential was held at 0.9 V and the flow rate of N_2 increased to 150 sccm (standard cubic centimetres of gas per minute) to ensure that all of the CO has been removed from the system. It has been found during the course of this work, and during related electrochemical studies, that the action of exposure of CO to platinum and the subsequent removal of that CO by electrochemical stripping is an excellent method of cleaning and activating the platinum [18]. No degradation of the catalytic performance of the MEA or the surface area of the platinum was noted during the course of these experiments.

When assessing surface area coverage based on the oxidative desorption of CO, a value of 420 μC cm^{-2} for polycrystalline Pt was employed [19].

In addition to CO, other components could potentially be distinguished at the electrode surface using this technique. Just as CO poisons platinum catalyst, sulphur containing species can be even more detrimental to fuel cell operation. The effect of sulphur on the performance of fuel cells has not been studied to the same extent as that of CO. Despite specific processing to remove sulphur from the fuel gas, it will still be present in trace quantities that can have an effect on performance. In the case of sulphur containing species, quantitative assessment of the level of coverage can be assessed from the oxidative stripping peak [20,21], or (as for CO) the suppression of the hydrogen upd peaks [22].

3. Results and discussion

3.1. The effect of flow rate on the adsorption of CO in a single channel

The two key parameters considered in this study are the effect of the carrier gas flow rate and the amount of CO injected. Assuming that the fuel cell is physically homogeneous, i.e. the catalyst is evenly dispersed; the GDL is of even thickness, porosity and composition; and the fuel cell is isothermal, three factors will determine where the CO is dispersed. These are the advective transport component along the channel; diffusion within the GDL (driven by a concentration gradient); and the local level of CO coverage of the catalyst. Under the temperature and pressure conditions applied in this study, the sticking probability of CO on platinum is expected to be close to 1 (for surface coverage less than saturation) [23]. Therefore, the presence of a sufficient quantity of CO in a given area of the MEA will be expected to quickly saturate the catalyst. Under such circumstances, the extent of poisoning at any particular position will be expected to be a function of CO concentration and residence time at that point. Of course, the reactant is effectively consumed when it chemisorbs onto the catalyst, therefore this technique not only represents a measure of exactly where gas will be distributed by natural diffusion and advection, but more importantly it provides a measure of where the catalyst will actually be poisoned in normal fuel cell operation.

The results described in this report are derived from integrated voltammetric stripping peaks and the timing of transient currents during the adsorption of CO. To aid quantitative comparison, our discussion concentrates on these derived values and does not consider the voltammetry in detail. Fig. 2(a) illustrates the various stages of the measurement. Starting with a flow of pure nitrogen, a dose of CO is added into this stream and the adsorption transient recorded. Following the injection of CO into the N_2 stream

and a suitable delay the voltage is swept at $10\,mV\,s^{-1}$ to 0.9 V and the stripping voltammogram is recorded.

During the CO adsorption process, a transient positive current is observed, Fig. 2(b). This current is not due to the oxidation of any CO, but rather due to the displacement of adsorbed hydrogen by CO, as the latter is a much stronger adsorbate:

$$Pt\text{-}H_{ad} + CO \rightarrow Pt\text{-}CO_{ad} + H^+ + e^- \quad (1)$$

In the main part of Fig. 2(b) the adsorption transient for the entire fuel cell (i.e. the sum of the current from each of the segments) is displayed as a function of the flow rate of the carrier gas along the channel for a CO injection volume of $0.2\,cm^3$. As the flow rate of the carrier gas is increased, the half-width of the adsorption transient increases, and the peak current shifts to later time. This result is initially counter-intuitive—it might be expected that as the residence time of the CO decreases with increasing flow rates, the peak width should be narrower, and the maximum current time should occur at earlier times. However, it should be realised that there are two transport mechanisms operating simultaneously—the first is advective transport along the channel, the second is diffusive transport through the gas diffusion layer in a direction perpendicular to the channel. Although diffusion is slower than advection at the flow rates used in these experiments (2 sccm is equivalent to an average flow velocity of $33\,mm\,s^{-1}$), both the cross-sectional area, and the amount of catalyst accessible by diffusion is much larger than is accessible by advection. For the entire length of channel studied in this paper, the cross-section of the diffusion layer is $37\,mm^2$ (110 mm channel length × 2 sides × 170 μm thick Toray™ paper GDL) versus a cross-section of only $1\,mm^2$ for the channel itself. We may envisage that during an experiment a "front" of CO rich gas moves over the surface of the MEA. In the region ahead of this front lie catalyst areas without any CO adsorbed on them, and behind the front lies catalyst areas on which CO has adsorbed. This "front" moves by either advection along the channel, or diffusion perpendicular to the direction of the channel. The rate of CO adsorption is related to the product of the speed at which the CO containing "front" of gas moves over the MEA with the length of the boundary between the CO occluded and CO-free catalyst areas. For the diffusional process, this boundary may be as long as the wall length of the channel (220 mm). In comparison, for the advection process, this boundary is the channel width, i.e. 1 mm. Thus as low flow rates favour the diffusion process, this allows access to much larger amounts of CO-free catalyst and thus the rate of adsorption is faster, and occurs at shorter time. At higher flow rates, the CO adsorption process relies on advection down the channel to bring the CO to fresh Pt sites, and this process provides a slower removal rate of CO compared to the former case. Displayed inset into Fig. 2(b) is the position sensitive variation of the adsorption current with time for the case of a 4 sccm flow rate of gas down the channel. A swift onset is observed for the localised adsorption transient followed by a sharp peak and a much slower subsequent decay. The initial time at which this onset occurs is staggered with position along the channel, and corresponds to an apparent front velocity of $1.06 \pm 0.05\,cm\,s^{-1}$, much slower than the average speed of the gas along the channel ($6.67\,cm\,s^{-1}$). The reason for this discrepancy is that as the 'plug' of CO moves along the channel, the leading edge of that plug is eroded due to CO adsorption and lateral diffusion of the CO into the gas diffusion layer adjacent to the channel. This results in a front which moves much slower than the average flow speed of the inert nitrogen flowing through the channel.

The distribution of the resulting adsorbed CO was then studied by electrochemically stripping the CO from the Pt surface using linear scan voltammetry. Fig. 2(c) shows the stripping voltammograms for the three different cases studied in Fig. 2(b). The stripping voltammograms all show a similar shape, but the total amount of CO adsorbed (i.e. the area under the peaks) decreases as the flow rate of gas through the channel increases. This effect occurs because at higher flow rates, some of the CO may get flushed out of the channel before it has a chance to adsorb onto a free Pt site. This aspect is more fully examined below. Displayed inset to Fig. 2(c) is the position sensitive variation in CO stripping voltammograms for the 4 sccm case in the main diagram. From the main diagram (Fig. 2(c)), it is obvious that all of the potential Pt adsorption sites are not taken (i.e. the integrated charge at lower flow rates is greater), hence it is not unexpected that some variation in the shape and size of the CO stripping peaks are seen as a function of position along the channel. The stripping peak at the beginning of the channel is the largest, and covers the widest potential range—this is consistent with the beginning of the channel being exposed to the CO pulse for a longer period of time. Further along the channel, the stripping voltammogram changes, decreasing in size, and with the peak shifting to higher potentials. This latter effect is consistent with CO initially binding to sites with a higher adsorption energy, or due to a change in the preferred sites of CO adsorption on Pt as has also been seen during experiments in our laboratories involving the oxidation of sub-saturation quantities of CO on Pt in sulphuric acid electrolyte.

In order to more fully understand the amount of CO which is lost due to being flushed out of the channel before it has a chance to adsorb at free Pt sites, we examined the effect of flow rate and CO injection volume on the proportion of CO adsorbed, Fig. 3. Under no circumstances is all of the CO adsorbed, instead the maximum amount is about 85% of the CO injected. The proportion of CO adsorbed decreases both as the amount of CO injected and the flow rate increase. This is what would be expected if the CO is being lost out of the cell via advection along the channel. Also plotted in Fig. 3 is a line corresponding to the theoretical residence time of the CO in the channel assuming the gas flow is laminar through a well defined square channel of $0.01\,cm^2$ cross-section—this calculation ignores the effects of CO adsorption and any interaction with the gas diffusion layer. It can be seen that the

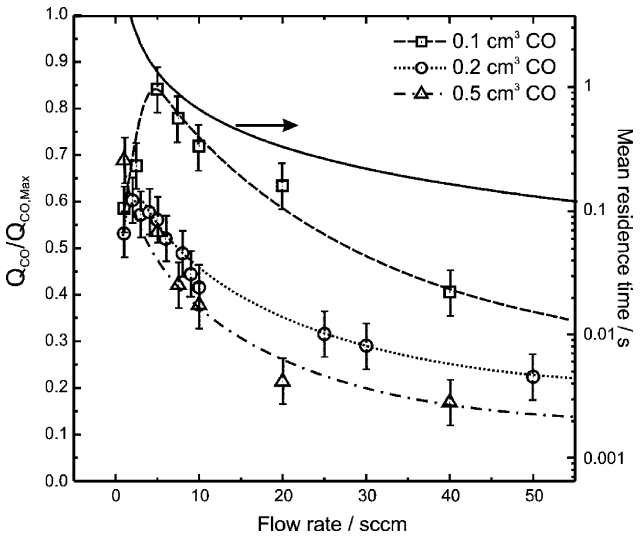

Fig. 3. Total CO stripping charge normalised against the maximum possible stripping charge vs. carrier gas flow rate. CO injections of 0.1, 0.2 and 0.5 cm^3 are shown along with the residence time of the carrier gas in the channel (solid line).

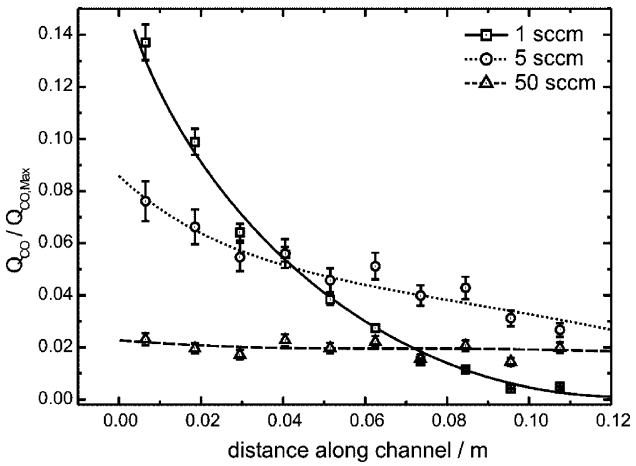

Fig. 4. Localised CO stripping charge normalised against the maximum possible stripping charge as a function of distance along the channel for flow rates of 1, 5 and 50 sccm. In all cases a 0.2 cm^3 volume of CO was injected into the channel.

residence time within the entire channel increases rapidly at flow rates less than 10 sccm. It will be shown later that it is within this region of flow rates that catalyst poisoning is most marked and leads to the most disparate distribution of adsorbed CO within the fuel cell. Surprisingly, there is also a decrease in the proportion of CO adsorbed at very low flow rates and CO injection volumes. This loss does not fit the above explanation, and instead we believe it is due to the lateral loss of CO via diffusion through the gas diffusion medium in a direction perpendicular to the channel. When advection along the channel is slow (i.e. at low flow rates), diffusion through the gas diffusion medium may compete and may become the principle transport mechanism for CO. Eventually some of the CO diffusing through the gas diffusion medium will reach the edge of the MEA and be lost. This effect is not so significant with larger volumes of injected CO as the amount of CO lost through this lateral diffusion mechanism is small and only weakly dependent of the amount of CO introduced into the channel—thus for larger injected volumes of CO the proportion of CO lost through this mechanism becomes negligible.

This argument is further strengthened by localised measurements. Fig. 4 shows the localised measurements of CO stripping charge with position following the injection of 0.2 cm^3 of CO into the channel whilst nitrogen was flowing at either 1, 5 or 50 sccm. The charge is normalised to the total charge which would be obtained if all of the CO were oxidised—thus the sum of all of the values for a given flow rate in Fig. 4 correspond to a single point in Fig. 3. It is seen in Fig. 4 that the CO stripping charge (and thus the CO distribution) is highly non-linear at low flow rates. Indeed, at the lowest flow rate virtually no CO is seen at the end of the channel. As the flow rate along the channel is increased, the distribution becomes more uniform, and at the highest flow rate, 50 sccm, the CO distribution is more or less independent with position. This result shows that lateral diffusion of reactants can dominate reactant transport, especially at low flow rates.

The data in Fig. 4 is re-plotted in Fig. 5 in which we use the information about the amount of CO adsorbed to develop a map of where it is adsorbed. It is important to note that Fig. 5 is derived from experimental results, and does not come about from any sort of simulation. Such a map may be very useful in understanding the pattern of poisoning within an operating fuel cell or in understanding the balance between reactant advection and diffusion in an operating fuel cell. In Fig. 5 we presume that the local coverage of CO on the Pt surface in the catalyst layer is either zero or is at a saturation value close to one. This is a reasonable assumption as at the temperature of these experiments the CO has a sticking coefficient very close to one for low coverages of CO [24]—thus once CO adsorbs on a free Pt site it does not desorb. Hence any free gaseous CO will very quickly adsorb onto any free Pt sites, and we will have a sharp transition between those areas with CO adsorbed on them (with saturation coverage) and those without any CO adsorbed (over which no CO has passed). We presume the distribution is symmetrical about the channel, and that the distribution is smooth (i.e. the distribution is interpolated between our experimental data points). Furthermore, in order to convert the CO stripping charge into coverage, we need to know the roughness factor of the platinum catalyst layer (i.e. the ratio of real Pt surface area to geometrical electrode surface area). A measure of the actual surface area of the platinum was obtained by integrating the charge associated with hydrogen underpotential deposition and removal obtained from voltammetry and correlated with the established value of 210 $\mu C\,cm^{-2}$ for polycrystalline Pt [25]. From this, the roughness factor of the catalyst layer (0.36 mg Pt cm^{-2})

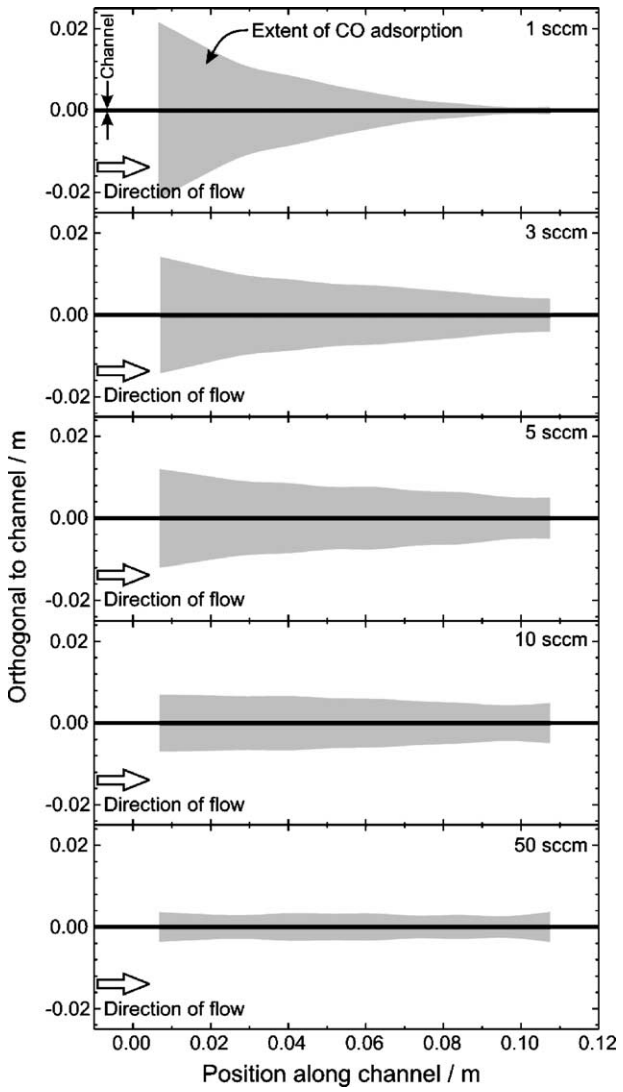

Fig. 5. CO adsorption distribution derived from the localised stripping charge for a CO dose of 0.2 cm^3. The orthogonal distance away from the centre of the channel into the GDL is shown with respect to the distance along the channel for flow rates of 1, 3, 5, 10 and 50 sccm.

was determined to be 130 ± 20. This means that, if all of the 0.2 cm^3 of CO is deposited on the catalyst in our MEA in such a way that the coverage is at saturation, then 67% of the MEA will be covered. The adsorbed CO distribution can then be calculated using the charge distribution along the channel, the roughness factor, and the charge associated with stripping one saturated monolayer of CO (420 $\mu C\,cm^{-2}$).

Fig. 5 is drawn to scale with the position and width of the channel (through which the CO and inert gas flow) highlighted. It is obvious that at all flow rates examined, the CO diffuses several channel widths distance from the channel through which it is flowing. It is clear that the extent of CO adsorption at different positions along the channel has a strong dependence on flow rate, with low flow rates exhibiting a highly anisotropic distribution. For low flow rates, where the residence time is higher, the CO has more time at any point along the channel to diffuse into the GDL. At 1 sccm most of the CO stripping charge is located towards the start of the channel with hardly any detected at the end. This is because most of CO is adsorbed in the early parts of the channel, due to the time afforded for it to diffuse into the GDL, and the flow of carrier gas is depleted of CO by the time it reaches the far end of the channel. At 50 sccm, the distribution is effectively uniform along the length of the channel, since the amount of CO in the channel is not significantly depleted as a function of position along the channel. However, the total extent of CO adsorption (i.e. the total area coloured grey) is much less than in the low flow case, since the low residence time does not allow sufficient time for the CO to diffuse into the GDL and adsorb.

It was previously commented upon in Fig. 3 that at low flow rates there is a net decrease in the amount of CO adsorbed, counter to what might be expected. As can be seen in the top diagram of Fig. 5, the CO distribution at low flow rates spreads all of the way to the edge of the MEA, and under these conditions CO will be lost "off the edge" of the MEA.

3.2. The effect of CO injection volume on adsorption of CO in a single channel

In addition to flow rate, the amount of CO exposed to the fuel cell is also expected to have a significant effect on where and to what extent CO adsorption occurs. To study this, the fuel cell was subjected to a range of CO doses, at flow rates of 2, 10 and 50 sccm. The ratio between the charge recovered during the electrochemical stripping of the CO divided by the maximum charge expected if all of the CO were adsorbed is then plotted against the volume of CO injected. Fig. 6 Line (b) in this diagram represents the relative charge

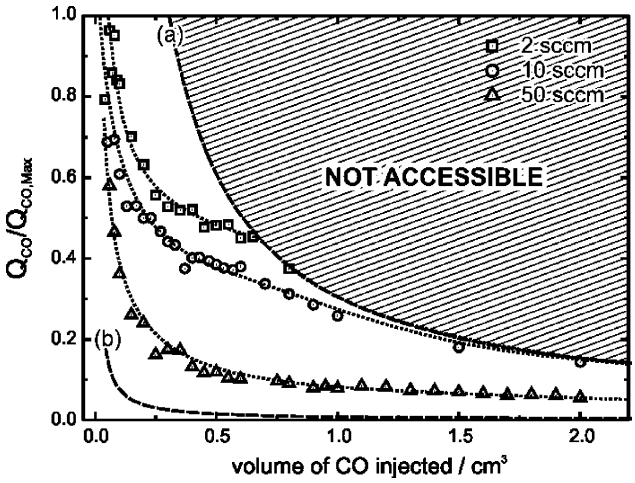

Fig. 6. Total CO stripping charge normalised against the maximum possible stripping charge vs. volume of CO injected at carrier gas flow rates of 2, 10 and 50 sccm. (a) Represents the boundary of the catalysed area of the MEA available for adsorption. (b) Represents the catalysed area of the MEA under the open face of the flow channel.

associated with CO adsorption in the catalyst layer immediately underneath the channel, i.e. the maximum relative charge expected if no lateral diffusion occurred. Line (a) represents the relative charge associated with CO covering all of the available Pt sites in the MEA, i.e. the case where lateral diffusion transports CO to all parts of the MEA. Obviously it is not possible to have relative charges greater than line (a), as there are no extra sites available for adsorption of the excess CO.

Several factors are of note in this figure. Complete utilisation of the entire amount of CO injected is only observed for the smallest dosage, and deviation from the maximum occurs most rapidly at higher flow rates, in agreement with the results presented in Fig. 3. At the lowest flow rate of 2 sccm, deviation from the maximum relative adsorption of CO occurs for injected amounts larger than ca. 0.1 cm^3, whereas at higher flow rates, there is no plateau, and the relative amount of adsorbed CO continuously decreases with increasing injection volume. The effect of flow rate has already been discussed and the same argument can be applied here to explain the difference between the three flow rates. That is, increased flow rate lowers the residence time in the channel, decreasing the ability of the CO to diffuse laterally and resulting in more CO transiting the entire channel and exiting into the exhaust. At low flow rates, as the volume of injected CO increases, there comes a point at which the relative amount of CO adsorbed reaches saturation, and the curves undergo a change in shape and follows curve (a). It should be borne in mind that each point in Fig. 6 represents the relative CO charge for the entire channel. In our case we can measure the local charge associated with CO stripping at different positions along the channel, and so can use our position sensitive data to convert that data to maps of CO coverage as a function of the volume of CO injected. In Fig. 7 we overlay each of the distributions associated with different CO injection volumes, for three different flow rates examined. It can be seen that at a given flow rate as the volume of CO injected increases, the area covered by the CO increases in a monotonic fashion. Some ripples in the boundaries are evident, and these are artefacts due to the smoothing and interpolation of the lines calculated from our experimental data.

Considering the profile of the 2 sccm case first, three different regimes of operation are observed at this flow rate, small volumes of CO only allow this reactant to diffuse into the GDL at the start of the channel; the latter portion of the channel only shows evidence of CO adsorption on the catalyst directly under the channel. As the volume of CO injected increases a distribution with an approximately constant gradient is observed along the length of the channel/GDL. At 0.8 cm^3 injected CO and above, virtually the entire MEA is saturated and the profile of CO adsorption becomes constant at ca. 2 cm from the channel, i.e. the edge of the catalysed area. Increasing the flow rate to 10 sccm, it is seen that an approximately constant gradient of distribution is observed over the range of dosage applied except at the highest dose of 2 cm^3 where the distribution is seen to

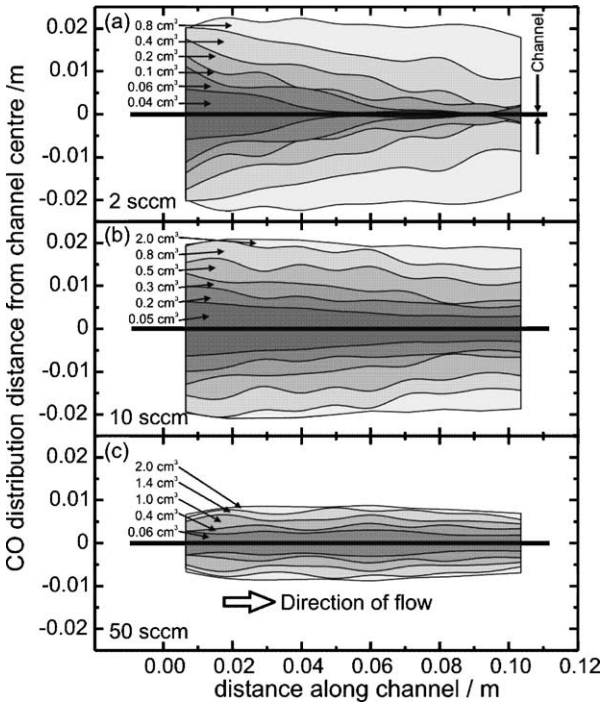

Fig. 7. CO adsorption distribution derived from the localised stripping charge for varying CO dosage at a carrier gas flow rate of 2, 10 and 50 sccm. The orthogonal distance away from the centre of the channel into the GDL is shown with respect to the distance along the channel.

flatten at 2 cm from the channel, as the entire catalyst area becomes saturated. At the highest flow rate of 50 sccm, a much flatter distribution profile is observed across the range of doses and saturation to the edge of the catalyst is not observed. Again, this is a consequence of less CO being adsorbed and more of it being swept through the channel to the exhaust at the higher flow rate.

Furthermore, the diagrams in Fig. 7 also provide information about the time-evolution of reactant transport through our fuel cell system. Each increase in the volume of CO injected into the channel is equivalent to the result which would be obtained if we could 'freeze' the fuel cell during the injection of a large volume of CO—they thus act as 'snap-shots' of how a front of reactant would pass both along the channel and laterally through the gas diffusion medium. The most interesting effect evident from this approach is that at channel low flow rates there is a significant diffusional component in the same direction as the convective flow in the channel. This is indicated by the angle which the boundaries make with the channel (on average 7°, 3°, and about 0.1° for the 2, 10 and 50 sccm cases, respectively). At high flow rates (Fig. 7(c)), the boundary is almost parallel to the channel.

4. Conclusion

This work has shown how localised stripping and adsorption transients can be used to ascertain the extent and location of CO distribution in an idealised single-channel fuel

cell. CO was used as a probe molecule because it is a poison within reformate fuelled fuel cells and is strongly adsorbed onto platinum at a potential at which it does not react. The latter is important as it allows us to decouple reactant transport from the oxidation of the adsorbed CO. In terms of the transport of molecules within a fuel cell we see two separate mechanisms competing with each other in determining the reactant distribution—the first is advection along the channel, the second is lateral diffusion perpendicular to the channel. Because of the simple geometry of our fuel cell system—a single channel with catalysed areas extending a distance of 2 cm from the channel, it is possible to study the latter process in greater detail than within a real fuel cell. At low reactant flow rates (<5 sccm in our configuration), lateral diffusion of reactants away from the channel becomes very significant. Thus it has been shown that for our simple cell flow-field geometry it is possible to correlate the residence time of the CO probe pulse with the localised stripping charge, to determine the extent of lateral diffusion through the GDL. By varying the volume of CO injected into the channel, and determining the resulting adsorbed CO distribution, it is possible to produce a set of 'snap-shots' of how the CO disperses both along the channel and laterally through the gas diffusion layer under different conditions.

Acknowledgements

The authors acknowledge a grant from the Engineering and Physical Sciences Research Council (GR/M73552) for partial support of this work. We also thank Johnson Matthey for the provision of the MEAs.

References

[1] P. Hoffmann, Tomorrow's Energy, Hydrogen, Fuel Cells and the Prospect for a Cleaner Planet, The MIT Press, Massachusetts, USA, 2001.
[2] D.J.L. Brett, S. Atkins, N.P. Brandon, V. Vesovic, N. Vasileiadis, A.R. Kucernak, Electrochem. Comm. 3 (2001) 628.
[3] D.J.L. Brett, S. Atkins, N.P. Brandon, V. Vesovic, N. Vasileiadis, A.R. Kucernak, Electrochem. Solid-State Lett. 6 (2003) A63–A66.
[4] S.J.C. Cleghorn, C.R. Derouin, M.S. Wilson, S. Gottesfeld, J. Appl. Electrochem. 28 (1998) 663.
[5] J. Stumper, S.A. Campbell, D.P. Wilkinson, M.C. Johnson, M. Davis, Electrochim. Acta 43 (1998) 3773.
[6] Ch. Wieser, A. Helmbold, E. Gülzow, J. Appl. Electrochem. 30 (2000) 803.
[7] M. Noponen, T. Hottinen, T. Mennola, M. Mikkola, P. Lund, J. Appl. Electrochem. 32 (2002) 1081.
[8] J. Ihonen, F. Jaouen, G. Lindbergh, G. Sundholm, Electrochim. Acta 46 (2001) 2899.
[9] M.M. Mench, C.Y. Wang, J. Electrochem. Soc. 150 (2003) A79.
[10] J.R. Rostrup-Nielsen, K. Aasberg-Peterson, in: W. Vielstich, H.A. Gasteiger, A. Lamm (Ed.), Handbook of Fuel Cells, Fundamental Technology and Applications, vol. 3, John Wiley and Sons Ltd., 2003, p. 159.
[11] J.R. Ladebeck, J.P. Wagner, in: W. Vielstich, H.A. Gasteiger, A. Lamm (Ed.), Handbook of Fuel Cells, Fundamental Technology and Applications, vol. 3, John Wiley and Sons Ltd., 2003, p. 190.
[12] S. Gottesfeld, J. Pafford, J. Electrochem. Soc. 135 (1988) 2651.
[13] D.P. Wilkinson, J. St-Pierre, J. Power Sources 113 (2003) 101.
[14] H. Dohle, R. Jung, N. Kimiaie, J. Mergel, M. Muller, J. Power Sources 124 (2003) 371.
[15] A. de Souza, E.R. Gonzalez, J. Solid State Electrochem. 7 (2003) 651.
[16] J. Soler, E. Hontanon, L. Daza, J. Power Sources 118 (2003) 172.
[17] A. Kumar, R.G. Reddy, J. Power Sources 113 (2003) 11.
[18] A. Palmer, Department of Chemistry, Imperial College, 2001, personal communication.
[19] A. Essalik, K. Amouzegar, O. Savagogo, J. Appl. Electrochem. 25 (1995) 404.
[20] N. Batina, J.W. McCargar, G.N. Salaita, F. Lu, L. Laguren-Davidson, C.-H. Lin, A.T. Hubbard, Langmuir 123 (1989) 123.
[21] D.-T. Chin, P.D. Howard, J. Electrochem. Soc. 133 (1986) 2447.
[22] Y.-E. Sung, W. Chrzanowski, A. Zolfaghari, G. Jerkiewicz, A. Wieckowski, J. Am. Chem. Soc. 119 (1997) 194.
[23] J.W. Bauman, T.A. Zawodzinski Jr., S. Gottesfeld, in: S. Gottesfeld, T.F. Fuller (Ed.), Proton Conducting Membrane Fuel Cells II, The Electrochemical Society Proceedings Series, Pennington, NJ, 1998, PV 98–27, p. 136.
[24] G.B. Hoflund, R.E. Gilbert, O. Melendez, React. Kinetics Catal. Lett. 52 (1994) 357–365.
[25] F.C. Nart, W. Vielstich, in: W. Vielstich, H.A. Gasteiger, A. Lamm (Ed.), Handbook of Fuel Cells, Fundamental Technology and Applications, vol. 2, John Wiley and Sons Ltd, 2003, p. 302.